Non-Darcy behavior in two-phase channel flow

Xianmin Xu[1,*] and Xiaoping Wang[2,†]

[1] *LSEC,Institute of Computational Mathematics and Scientific/Engineering Computing, NCMIS, AMSS, Chinese Academy of Sciences, Beijing 100190, China*

[2] *Department of Mathematics, Hong Kong University of Science and Technology, Clear Water Bay, Kowloon, Hong Kong, China*

We study the macroscopic behavior of two phase flow in porous media from a phase filed model. A dissipation law is first derived from the phase field model by homogenization. For simple channel geometry in pore scale, the scaling relation of the averaged dissipation rate with the velocity of the two phase flow can be explicitly obtained from the model which then gives the force-velocity relation. It is shown that for the homogeneous channel surface, Dacry's law is still valid with an significantly modified permeability including the contribution from the contact line slip. For the chemically patterned surfaces, the dissipation rate has a non-Darcy linear scaling with the velocity, which is related to a depinning force for the patterned surface. Our result offers a theoretical understanding on the prior observation of non-Darcy behavior for the multi-phase flow in either simulations or experiments.

I. INTRODUCTION

The study of porous media flow is of critical importance in many applications such as petroleum industry, soil sciences, fuel cells, painting filtration, etc. One-phase flow in porous media is well understood so far. Darcy law, first derived through experiments in the 19th century[1], represents a linear relationship between the filtration velocity $\mathbf{v}$ and the pressure gradient: $\mathbf{v} = -K\nabla p$. The Darcy law can also be rigorously derived from Navier-Stokes equations by homogenization techniques [2–4] or the volume averaging method[5–7]. Nonlinear corrections to the Darcy law have been studied under various situations (see [8, 9] and reference therein).

The modeling of two phase flows in porous media has been mostly based on empirical approaches[10], with assumed analogy with single phase flow. In particular, with $\mathbf{v}_i$ being the superficial or seepage velocity vector of phase i relative to the fixed pores, the two-phase form of the Darcy law is taken to be

$$\mathbf{v}_i = -\frac{k_{ri}}{\eta_i} K(\nabla p_i - \rho_i \mathbf{g}), \quad \frac{\partial s_i}{\partial t} + \nabla \cdot (s_i \mathbf{v}_i) = 0, \quad (1)$$

where k_{ri} represents the relative permeability of phase i, $i = 1, 2$, and $p_1 - p_2 = p_c$ defines the capillary pressure. Both k_{ri} and p_c are assumed to be dependent only on the saturations $s_i (s_1 + s_2 = 1)$, and the explicit functional relationships are assumed to be known from experiments.

Although the above model has been widely used in petroleum engineering, soil science, as well as many other fields, it has long been argued that the model might be invalid either by theory, experiments, or both. Shortcomings of the model include: no account of interfacial force being taken in the momentum equation; and quasi-static capillary pressure curves were used for highly dynamic flow process. Due to the complexity of two-phase flow in porous media, most of studies concern mainly the pure imbibition or pure drainage process, where a macroscopic fluid interface moving across porous media flow (see for example [11]). There are also many experimental or numerical studies on porous media flow for a pore-network model. Among them, Avraam *et al.* did extensive experiments to show how the (conventional and generalized) relatively permeabilities depend on various regimes of flow mechanics, the capillary number, the flow ratio and the viscosity ratio, etc[12–14]. Recently, Tallakstad *at el.* carried out some interesting experiments on steady two-phase flow in a representative porous media volume, where two phases are mixed together and both drainage and imbibition interplays[15, 16]. They report some highly nontrivial behavior of the pressure jump with respect to capillary number.

In this paper, we study the macroscopic behavior of two-phase immiscible flow in the porous media, using a phase field model with generalized Navier boundary condition developed in [17, 18]. Using homogenization technique, we first derive a generalized macroscopic dissipation law, $\mathcal{R}(\mathbf{x}) = -\nabla P(\mathbf{x}) \cdot \mathbf{U}(\mathbf{x})$, that is valid for multiphase flows in porous media. We then use the dissipation law to study the effect of contact lines and roughness of pore surfaces on the macroscopic behavior of the two-phase flow by considering some simple pore geometries. For two phase Poiseuille flow in a homogeneous channel, our calculations show that the Darcy's law still holds with the permeability significantly reduced due to the dissipation associated with the contact line slip. The analysis is consistent with the Tallakstad experiments [15, 16]. We then consider the case in which the channel surface is chemically patterned. It is shown that the total dissipation displays the scaling behavior $\mathcal{R} = FU \propto F_0 U + \lambda U^2$ which includes a non-Darcy term $F_0 U$ that arises from the surface inhomogeneities. This non-Darcy term gives the force-velocity relation $U \propto (F - F_0)$ for the chemically patterned surfaces.

We would like to remark that the simple pore geometry assumption ignores the interaction of different layers and

* xmxu@lsec.cc.ac.cn

† mawang@ust.hk

high dimensional effect. However, our analysis provides some new theoretical understanding of the Darcy's and Non-Darcy's behaviour in two-phase flow in porous media induced by the extra dissipations near moving contact lines. The dependence of the permeability and the depinning force on the behavior of the moving contact lines is quantitatively shown. We expect the force-dissipation relation and the analysis in this paper will be helpful in further studies in general porous media geometry.

The structure of the paper is as follows. In Section II, we carry out homogenization analysis for a non-dimensionalized two-phase flow model in porous media. A macroscopic dissipation relation is derived. In Section III, we analyse in detail the case when the pore is a channel. Some general discussions are provided to show the difference of our results with standard Leverett models. The generalization to higher dimensional case is briefly discussed. In Section IV, numerical experiments are illustrated and verify the analysis in the previous section. Finally, we give a few conclusion remarks in Section V.

II. MACROSCOPIC DISSIPATION FOR THE TWO-PHASE FLOW IN POROUS MEDIA

In [17], the Cahn-Hilliard-Navier-Stokes(C-H-N-S) equations with the generalized Navier boundary condition (GNBC) are proposed to described the behavior of the moving contact line:

$$\begin{cases} \frac{\partial \phi}{\partial t} + \mathbf{v}\cdot\nabla\phi = M\Delta\mu, \\ \rho[\frac{\partial \mathbf{v}}{\partial t} + (\mathbf{v}\cdot\nabla)\mathbf{v}] = \mathbf{F} - \nabla p + \eta\Delta\mathbf{v} + \mu\nabla\phi, \\ \nabla\cdot\mathbf{v} = 0. \end{cases} \tag{2}$$

The first equation is the Cahn-Hilliard equation considering the convection of the fluid. ϕ is the general phase field function. $\mu = -K\Delta\phi - r(\phi-\phi^3)$ is the chemical potential with the interface thickness $\xi = \sqrt{K/r}$ and the fluid-fluid interface tension $\gamma = 2\sqrt{2}r\xi/3$. M is a phenomenological mobility coefficient.

The second equation is the Navier-Stokes equation with additional term $\mu\nabla\phi$, the capillary force exerted to the fluid by the interface. For simplicity, we assume that the two fluids have the equal constant density ρ and viscosity η.

The boundary conditions for the phase field ϕ, the normal velocity and the chemical potential are given by

$$\begin{aligned} &\tfrac{\partial \phi}{\partial t} + v_\tau\partial_\tau\phi = -\Gamma L(\phi), \\ &v_n = 0,\ \partial_n\mu = 0, \end{aligned} \tag{3}$$

with Γ being a positive phenomenological parameter. v_n and v_τ are normal and tangential velocity, respectively. The Generalized Navier boundary condition is proposed to describe the moving contact lines:

$$\beta v_\tau = -\eta\partial_n v_\tau + L(\phi)\partial_\tau\phi, \tag{4}$$

Here β is a slip coefficient and the slip length is given as $\tilde{l}_s = \eta/\beta$. $L(\phi) = K\partial_n\phi + \frac{\partial\gamma_{wf}(\phi)}{\partial\phi}$, where $\gamma_{wf}(\phi) = -\frac{\gamma}{4}\cos\theta_s(3\phi-\phi^3)$ is the solid-fluid interface energy density (up to a constant) and θ_s is the static contact angle. $L(\phi)\partial_\tau\phi$ represents the uncompensated Young stress.

A. Non-dimensionalization

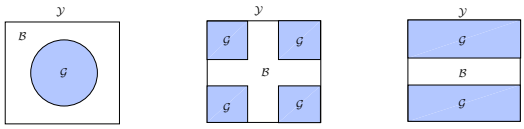

FIG. 1. Examples of cell structures in periodic porous media.

We consider two-phase flow in a porous media. Denote $\varepsilon = l/L$, the ratio between the pore length scale l and the macroscopic scale L. We then scale the velocity by the characteristic velocity v^*, the length by L, the time by L/v^*, body force(density) $\mathbf{F}$ by $\eta v^*/l^2$ and the pressure by $L\eta v^*/l^2$. With five dimensionless parameters,

$$\begin{aligned} &\mathsf{L_d} = \frac{3M\gamma}{2\sqrt{2}v^*l^2}, \mathsf{R_e} = \frac{\rho v^* l}{\eta}, \mathsf{B} = \frac{3\gamma}{2\sqrt{2}\eta v^*}, \\ &\mathsf{V_s} = \frac{3\gamma\Gamma l}{2\sqrt{2}v^*}, l_s = \frac{\tilde{l}_s}{l}, \delta = \frac{\xi}{l}, \end{aligned} \tag{5}$$

we have the following dimensionless Cahn-Hilliard-Navier-Stokes equations

$$\begin{cases} \frac{\partial \phi}{\partial t} + \mathbf{v}\cdot\nabla\phi = \varepsilon^2\mathsf{L_d}\Delta\mu, \\ \varepsilon\mathsf{R_e}\left[\frac{\partial \mathbf{v}}{\partial t} + (\mathbf{v}\cdot\nabla)\mathbf{v}\right] = \mathbf{F} - \nabla p + \varepsilon^2\Delta\mathbf{v} + \varepsilon^2\mathsf{B}\mu\nabla\phi, \\ \nabla\cdot\mathbf{v} = 0, \end{cases} \tag{6}$$

where the chemical potential $\mu = -\varepsilon\delta\Delta\phi - \phi/(\varepsilon\delta) + \phi^3/(\varepsilon\delta)$. The boundary conditions are

$$\begin{cases} \varepsilon[\frac{\partial \phi}{\partial t} + v_\tau\partial_\tau\phi] = -\mathsf{V_s}\mathcal{L}(\phi), \\ l_s^{-1}v_\tau = -\varepsilon\partial_n v_\tau + \varepsilon\mathsf{B}\mathcal{L}(\phi)\partial_\tau\phi, \\ \nabla\mu\cdot\mathbf{n} = 0, \quad \mathbf{v}\cdot\mathbf{n} = 0, \end{cases} \tag{7}$$

where $\mathcal{L}(\phi) = \varepsilon\delta\nabla\phi\cdot\mathbf{n} + \frac{\partial\gamma_{wf}(\phi)}{\partial\phi}$ and $\gamma_{wf}(\phi) = -\frac{\sqrt{2}}{6}\cos\theta_s(3\phi-\phi^3)$ being the wall-fluid interface energy density function. $\mathbf{n}$ is the unit out normal on the boundary.

B. Homogenization results

We now derive the macroscopic behavior of the two phase flow in porous media by the homogenization procedures. Let $\Omega\subset\mathbb{R}^2$ be a bounded domain which contains the porous media under consideration. For simplicity, we assume the porous media comprise a periodic array of small cells with size $\varepsilon \ll 1$. Denote the unit cell as $\mathcal{Y}$, which can be decomposed into two domains $\mathcal{B}$ and $\mathcal{G}$(as

shown in Fig. 1). Consider the porous domain defined by the fluid part $\Omega^\varepsilon = \Omega \cap \varepsilon(\cup_{\mathbf{z}\in\mathcal{A}}(\mathbf{z}+\mathcal{B}))$. Here $\mathcal{A}$ is an infinite lattice in $\mathbb{R}^2$ such that $\cup_{\mathbf{z}\in\mathcal{A}}(\mathbf{z}+\mathcal{Y}) = \mathbb{R}^2$ and $(\mathbf{z}_1+\mathcal{Y})\cap(\mathbf{z}_2+\mathcal{Y}) = \varnothing$, for any $\mathbf{z}_1, \mathbf{z}_2 \in \mathcal{A}$.

We assume that the unknown velocity, pressure and phase field function have the following expansion,

$$\begin{aligned}
\mathbf{v}(\mathbf{x}) &= \mathbf{v}_0(\mathbf{x},\mathbf{y}) + \varepsilon\mathbf{v}_1(\mathbf{x},\mathbf{y}) + \varepsilon^2\mathbf{v}_2(\mathbf{x},\mathbf{y}) + \cdots,\\
p(\mathbf{x}) &= p_0(\mathbf{x},\mathbf{y}) + \varepsilon p_1(\mathbf{x},\mathbf{y}) + \varepsilon^2 p_2(\mathbf{x},\mathbf{y}) + \cdots,\\
\phi(\mathbf{x}) &= \phi_0(\mathbf{x},\mathbf{y}) + \varepsilon\phi_1(\mathbf{x},\mathbf{y}) + \varepsilon^2\phi_2(\mathbf{x},\mathbf{y}) + \cdots,
\end{aligned}$$

where $\mathbf{y} = \frac{\mathbf{x}}{\varepsilon}$. Assume $\mathbf{v}_i$, p_i and ϕ_i to be all periodic in $\mathbf{y}$.

It is easy to see that the differential operators

$$\nabla = \nabla_x + \varepsilon^{-1}\nabla_y, \qquad \Delta = \Delta_x + 2\varepsilon^{-1}(\nabla_x\cdot\nabla_y) + \varepsilon^{-2}\Delta_y,$$

where $\nabla_x = (\partial_{x_1}, \partial_{x_2})^T$ and $\nabla_y = (\partial_{y_1}, \partial_{y_2})^T$, and $\Delta_y = \partial_{y_1y_1} + \partial_{y_2y_2}$. Straightforward calculations show that the chemical potential μ can also be expanded as

$$\mu(\mathbf{x}) = \varepsilon^{-1}\mu_0(\mathbf{x},\mathbf{y}) + \mu_1(\mathbf{x},\mathbf{y}) + O(\varepsilon),$$

with

$$\begin{aligned}
\mu_0 &= -\delta\Delta_y\phi_0 - \phi_0/\delta + \phi_0^3/\delta,\\
\mu_1 &= -\delta(2\nabla_x\cdot\nabla_y\phi_0 + \Delta_y\phi_1) - \phi_1(1-3\phi_0^2)/\delta.
\end{aligned}$$

Similarly, we have

$$\mathcal{L}(\phi) = \mathcal{L}_0(\phi_0) + O(\varepsilon),$$

with $\mathcal{L}_0(\phi_0) = \delta\nabla_y\phi_0\cdot\mathbf{n} + \frac{\partial\gamma_{wf}(\phi_0)}{\partial\phi}$. In addition, we introduce the fast time variable $s = \frac{t}{\varepsilon}$ and assume all quantities f in the system to depend on s, i.e. $f = \phi_i, \mathbf{v}_i$ and is periodic in s with period T. From the definition, we have $\frac{\partial f}{\partial t} = \frac{1}{\varepsilon}\frac{\partial f}{\partial s}$.

Substitute the expansions into above equations (6)-(7)(see details in Appendix A.1). The leading order term of the second equation of (6) gives

$$\nabla_y p_0 = 0, \tag{8}$$

This implies that p_0 depends only on the slow parameter $\mathbf{x}$ and can therefore be taken to be the macroscopic pressure. To the leading order, the velocity, phase function and the chemical potential satisfy the following equations in the representative cell $\mathcal{Y}$ near $\mathbf{x}$,

$$\begin{cases}
\mathsf{R_e}[\frac{\partial\mathbf{v}_0}{\partial s} + (\mathbf{v}_0\cdot\nabla_y)\mathbf{v}_0] = \mathbf{F} - \nabla_x p_0 - \nabla_y p_1 + \Delta_y\mathbf{v}_0 \\
\qquad\qquad +\mathsf{B}\mu_0\nabla_y\phi_0, & \text{in } \mathcal{B}\\
\nabla_y\cdot\mathbf{v}_0 = 0, & \text{in } \mathcal{B}\\
\frac{\partial\phi_0}{\partial s} + \mathbf{v}_0\cdot\nabla_y\phi_0 = \mathsf{L_d}\Delta_y\mu_0, & \text{in } \mathcal{B}\\
\mathbf{y}\to\mathbf{v}_0, p_1, \phi_0, \text{periodic boundary condition on } \partial\mathcal{Y}\cap\partial\mathcal{B}.
\end{cases} \tag{9}$$

with the boundary conditions on $\partial\mathcal{G}\cap\partial\mathcal{B}$,

$$\begin{cases}
\frac{\partial\phi_0}{\partial s} + v_{0,\tau}\nabla_y\phi_0\cdot\tau = -\mathsf{V_s}\mathcal{L}_0(\phi_0),\\
l_s^{-1}v_{0,\tau} = -(\nabla_y v_{0,\tau}\cdot\mathbf{n}) + \mathsf{B}\ \mathcal{L}_0(\phi_0)\nabla_y\phi_0\cdot\tau,\\
\nabla_y\mu_0\cdot\mathbf{n} = 0, \quad \mathbf{v}_0\cdot\mathbf{n} = 0,
\end{cases} \tag{10}$$

with $\mathcal{L}_0(\phi_0) = \delta\nabla_y\phi_0\cdot\mathbf{n} + \frac{\partial\gamma_{wf}(\phi_0)}{\partial\phi}$, and $\mu_0 = -\delta\Delta_y\phi_0 - \phi_0/\delta + \phi_0^3/\delta$.

We define $P(\mathbf{x}) = p_0(\mathbf{x})$ as the macroscopic pressure. Notice that since $\mathbf{v}_0$ is periodic in time s with period T, the macroscopic velocity can be defined as

$$\mathbf{U}(\mathbf{x}) = \frac{1}{T|\mathcal{B}|}\int_0^T\int_{\mathcal{B}}\mathbf{v}_0 \mathrm{d}\mathbf{y}\mathrm{d}s$$

with $|\mathcal{B}|$ being the volume of $\mathcal{B}$. In the case of one phase, low Reynolds number flow, the macroscopic velocity can be solved from a simplified equation similar to the first equation in (9), in terms of the pressure gradient. The usual one phase Darcy law then follows, where the permeability is expressed in terms of the solution of a cell problem. However, such derivation does not work for the two phase system (9). We show, however, that a dissipation law is still valid.

C. Dissipation function and the Darcy law

We multiply $\mathbf{v}_0$ to the first equation of (9) and integrate in $\mathcal{B}$. Direct computations give (see Appendix A.2)

$$\big(\mathbf{F} - \nabla P(\mathbf{x})\big)\cdot\mathbf{U}(\mathbf{x}) = \mathcal{R}(\mathbf{x}), \tag{11}$$

where

$$\begin{aligned}
\mathcal{R}(\mathbf{x}) =& \frac{1}{T|\mathcal{B}|}\Big[\int_0^T\int_{\mathcal{B}}|\nabla\mathbf{v}_0|^2\mathrm{d}\mathbf{y}\mathrm{d}s + \int_0^T\int_{\partial\mathcal{G}}\frac{v_{0,\tau}^2}{l_s}\mathrm{d}\sigma_y\mathrm{d}s\\
&+ \frac{\mathsf{B}}{\mathsf{V_s}}\int_0^T\int_{\partial\mathcal{G}}\dot{\phi_0}^2\mathrm{d}\sigma_y\mathrm{d}s + \mathsf{BL_d}\int_0^T\int_{\mathcal{B}}|\nabla\mu_0|^2\mathrm{d}\mathbf{y}\mathrm{d}s\Big].
\end{aligned} \tag{12}$$

is the averaged dissipation rate over a cell [18].

The macroscopic behavior is characterized by Eq. (11). If we know how the averaged dissipation rate depends on $\mathbf{U}$, then an explicit relation between the force $\mathbf{F}-\nabla P$ and $\mathbf{U}$ may be obtained. In particular, if $\mathcal{R}$ scales quadratically with $\mathbf{U}$(which is the case for the single phase flow), then the Darcy law is recovered.

In the following, we consider only the simplest channel geometry in pore scale. It is shown that the Darcy law form still holds for smooth wall surfaces (with a permeability changed significantly by the effect of moving contact lines), but deviation from the Darcy law occurs when the surfaces are inhomogeneous. In the latter case the dissipation function has precisely the form as given by $\mathcal{R} = FU \propto F_0U + \lambda U^2$.

III. TWO-PHASE CHANNEL FLOW

We consider a channel of length L_x and height h, i.e. $\mathcal{B} = \{(y_1,y_2)\in(0,L_x)\times(0,h)\}$ and denote the upper and lower boundary of the channel $\partial\mathcal{G} = \{y_2 = 0, h; 0 < y_1 < L_x\}$(see Fig. 2). The two phase flow in the channel

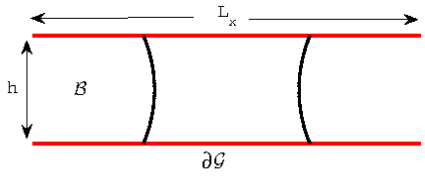

FIG. 2. Two phase flow in a channel with homogeneous upper and lower boundaries.

is modeled by the C-H-N-S equations (9) with boundary conditions (10). For simplicity, we use p, ϕ, $\mathbf{v}$, μ, $\mathbf{F}$, $\mathcal{L}$ and t instead of p_1, ϕ_0, $\mathbf{v}_0$, μ_0, $\mathbf{F}-\nabla_x p_0$, $\mathcal{L}_0$ and s, respectively. The equations are reduced to

$$\begin{cases} \mathsf{R_e}[\frac{\partial \mathbf{v}}{\partial t}+(\mathbf{v}\cdot\nabla)\mathbf{v}] = \mathbf{F}-\nabla p+\Delta\mathbf{v}+\mathsf{B}\mu\nabla\phi, \\ \nabla\cdot\mathbf{v}=0, \\ \frac{\partial\phi}{\partial t}+\mathbf{v}\cdot\nabla\phi = \mathsf{L_d}\Delta\mu, \\ \mathbf{y}\to \mathbf{v}, p, \phi, \text{periodic boundary condition, on} \{y_1=0, L_x\} \end{cases} \tag{13}$$

with the boundary conditions on $\{y_2=0, h\}$,

$$\begin{cases} \frac{\partial\phi}{\partial t}+v_\tau\nabla\phi\cdot\tau = -\mathsf{V_s}\mathcal{L}(\phi), \\ l_s^{-1}v_\tau = -(\nabla v_\tau\cdot\mathbf{n})+\mathsf{B}\ \mathcal{L}(\phi)\nabla\phi\cdot\tau, \\ \nabla\mu\cdot\mathbf{n}=0, \quad \mathbf{v}\cdot\mathbf{n}=0, \end{cases} \tag{14}$$

with $\mu=-\delta\Delta\phi-\phi/\delta+\phi^3/\delta$ and $\mathcal{L}(\phi)=\delta\nabla\phi\cdot\mathbf{n}+\frac{\partial\gamma_{wf}(\phi)}{\partial\phi}$. All the differential operators in the equations are now with respect to $\mathbf{y}$. We assume the external force $\mathbf{F}$ to be a constant vector (with respect to $\mathbf{y}$) along the y_1 direction.

A. Homogeneous surfaces: Darcy law in the presence of the contact line

We now assume that the solid surface $\partial\mathcal{G}$ is chemically homogeneous. That is, θ_s is a constant along the boundary. With the constant external force $\mathbf{F}=(F_1,0)$ in the y_1 direction, we can assume that the system (13) and (14) admits a traveling wave solution of the form

$$\begin{aligned} \mathbf{v}(\mathbf{y},t) &= \mathbf{v}(\mathbf{y}-\mathbf{U}t), \\ p(\mathbf{y},t) &= p(\mathbf{y}-\mathbf{U}t), \\ \phi(\mathbf{y},t) &= \phi(\mathbf{y}-\mathbf{U}t), \end{aligned}$$

with a constant velocity $\mathbf{U}=(U,0)$. The system (6) and (7) are reduced to

$$\begin{cases} \mathsf{R_e}\Big[\big((\mathbf{v}-\mathbf{U})\cdot\nabla\big)\mathbf{v}\Big] = \mathbf{F}-\nabla p+\Delta\mathbf{v}+\mathsf{B}\mu\nabla\phi, & \mathbf{y}\in\mathcal{B}; \\ (\mathbf{v}-\mathbf{U})\cdot\nabla\phi = \mathsf{L_d}\Delta\mu, & \mathbf{y}\in\mathcal{B}; \end{cases} \tag{15}$$

and

$$(v_\tau-U)\partial_\tau\phi = -\mathsf{V_s}\mathcal{L}(\phi) \quad \mathbf{y}\in\partial\mathcal{G}. \tag{16}$$

We multiply $\mathbf{U}$ to the first equation of (15) and integrate in $\mathcal{B}$. We have, by direct computations(see Appendix A.3),

$$F|\mathcal{B}| = \int_{\partial\mathcal{G}} l_s^{-1}v_\tau \mathrm{d}\sigma_y. \tag{17}$$

This implies that the external body force is balanced by boundary frictions.

The profile of the slip velocity near the moving contact lines on the solid boundary has been studied previously [19–21]. The velocity profile is found to have a universal behavior, see more discussion in Appendix B., i.e., $\frac{v_\tau}{U}\approx g\big(\frac{d(\mathbf{y},\mathbf{y}_i)}{l_s}\big)$, where $d(\mathbf{y},\mathbf{y}_i)$ is the distance from $i-$th contact point $\mathbf{y}_i$, $g(\xi)$ is a universal function with a power-law slip region extending from a critical place about r_c away from the contact line. In [19], it is found that $g(\xi)=1/(1+\xi/a)$, with $a\approx 2.14$. The outer cutoff for the partial-slip region R is determined by the height h of the channel. Beyond the partial slip region, the slip velocity has a value given by $v_s=6l_sU/(h+6l_s)$ which can be derived from the Stokes equation for the single phase Poiseuille flow with Navier slip boundary condition. For each contact point $\mathbf{y}_i$, it is shown that $\int_{\partial\mathcal{G}\cap\{\mathbf{y}:d(\mathbf{y},\mathbf{y}_i)<\mathsf{R}\}} l_s^{-1}v_\tau\mathrm{d}\sigma_y\approx \mathsf{A}U$, with some constant A independent of U. The value of A depends on the size of power-law area. Thus, if we suppose that there are n contact points on each side of $\partial\mathcal{G}$, then

$$\int_{\partial\mathcal{G}} l_s^{-1}v_\tau\mathrm{d}\sigma_y \approx \Big(2n\mathsf{A}+\frac{12(L_x-2n\mathsf{R})}{h+6l_s}\Big)U \tag{18}$$

where $2n$ is the number of contact points in the pore.

It follows from (17) and (18) that

$$U=\frac{h(h+6l_s)}{12+2n(\mathsf{A}h+6l_s\mathsf{A}-12\mathsf{R})/L_x}F. \tag{19}$$

and the permeability is given by:

$$k=\frac{h(h+6l_s)}{12+2n(\mathsf{A}-\frac{12\mathsf{R}}{h+6l_s})\frac{h+6l_s}{L_x}}. \tag{20}$$

Notice that for the one phase flow, i.e. $n=0$, we recover the usual permeability expression for the slip boundary condition that $k_0=h(h+6l_s)/12$. In the presence of a contact line, however, the results in [19, 21] show that R is linearly proportional to h and A behaves as $\log(\mathsf{R}/l_s)$. Therefore the expression $2n(\mathsf{A}-12\mathsf{R}/(h+6l_s))(h+6l_s)/L_x$ (in the denominator of (19)), which represents the contribution from the partial slip dissipation near the contact line and which scales as $h/L_x\log(h/l_s)$ for h/l_s large, can significantly reduce the effective permeability. This is verified by our numerical experiments given in Table I.

From (20), the inverse of the permeability scales like

$$k^{-1}\approx k_0^{-1}(1+b\cdot n) \tag{21}$$

where k_0 is the standard permeability for one-phase porous media flow, n is the total number of contact points

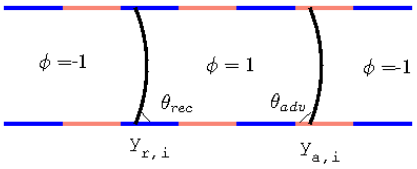

FIG. 3. Two phase flow in a channel with chemically patterned upper and lower boundaries(color online).

in a representative volume and $b \propto \log(h/l_s)h/L_x$, depending on both the geometry size and the slip-length of the two-phase flows.

B. Inhomogeneous surfaces: Non-Darcy behavior

We now consider two phase flow in a chemically patterned channel with the top and bottom surfaces patterned periodically (with small period, see Fig. 2) by two different materials with equal length but different contact angles θ_a and θ_b. Without the loss of generality, we assume $\theta_a > \theta_b$. We also assume that the motion of the two-phase flow is periodic in time with period T and denote the time averaged horizontal velocity as $U = \frac{1}{T|\mathcal{B}|}\int_0^T \int_{\mathcal{B}} v_1 \mathrm{d}\mathbf{y}\mathrm{d}t$. It is reasonable to assume that $\frac{1}{T|\mathcal{B}|}\int_0^T \int_{\mathcal{B}} v_2 \mathrm{d}\mathbf{y}\mathrm{d}t = 0$ in the channel. Multiply the first equation of (9) by $\mathbf{U} = (U, 0)$ and integrate in both space and time, we obtain

$$\mathbf{F}\cdot\mathbf{U}|\mathcal{B}| = \mathsf{Re}\int_{\mathcal{B}} \partial_t \mathbf{v}\cdot\mathbf{U} + (\mathbf{v}\cdot\nabla)\mathbf{v}\cdot\mathbf{U}\mathrm{d}\mathbf{y} - \int_{\mathcal{B}} (-\nabla p + \Delta\mathbf{v} + \mathsf{B}\mu\nabla\phi)\cdot\mathbf{U}\mathrm{d}\mathbf{y}. \quad (22)$$

By careful computations(see in Appendix A.3), the equation is reduced to

$$FUL_x hT = U\int_0^T\int_{\partial\mathcal{G}} l_s^{-1} v_\tau \mathrm{d}\sigma_y\mathrm{d}t - \frac{4\sqrt{2}}{3}\mathsf{B}U\int_0^T\int_{\partial\mathcal{G}} \cos\theta_s(y_1)\frac{\partial(3\phi-\phi^3)/4}{\partial y_1}\mathrm{d}y_1\mathrm{d}t. \quad (23)$$

For the first term on the right-hand side of (23), similar calculations as in homogeneous boundary case gives

$$\int_0^T\int_{\partial\mathcal{G}} l_s^{-1} v_\tau \mathrm{d}\sigma_y\mathrm{d}t \approx \Big(2n\mathsf{A} + \frac{12(L_x - 2n\mathsf{R})}{h + 6l_s}\Big)UT. \quad (24)$$

Unlike in the homogeneous surface case, the last term in the right-hand side of (23) no longer vanishes for the inhomogeneous surface, which is the origin of the non-Darcy effect. Assume the solution is symmetric along the channel height, we then have

$$\int_0^T\int_{\partial\mathcal{G}} \cos\theta_s(y_1)\frac{\partial(3\phi-\phi^3)/4}{\partial y_1}\mathrm{d}y_1\mathrm{d}t = 2\int_0^T\int_0^{L_x} \cos\theta_s(y_1)\frac{\partial(3\phi-\phi^3)/4}{\partial y_1}\mathrm{d}y_1\mathrm{d}t. \quad (25)$$

We estimate the above integral in the sharp-interface limit of the phase field function. When the interface thickness δ goes to zero, the phase field function ϕ converges to a step function switching values between 1 and -1. Due to the periodicity in y_1, the interfaces appear in pairs with one increasing from -1 to 1, which we define as "receding" interface, followed by one decreasing from 1 to -1, which we define as the "advancing" interface. The "advancing" and "receding" are with reference to the phase value $\phi = 1$(see Fig. 2). Thus in the sharp-interface limit we have $\frac{\partial(3\phi-\phi^3)/4}{\partial y_1} \approx \sum_{i=1}^n (\delta_{y_{r,i}(t)} - \delta_{y_{a,i}(t)})$, where $\delta_{y_{r,i}(t)}$ and $\delta_{y_{a,i}(t)}$ are Dirac functions, $y_{r,i}(t)$ and $y_{a,i}(t)$ are the y_1 coordinates of the i-th receding and i-th advancing contact points on $\partial\mathcal{G}$ at time t, respectively. Due to periodicity of the system, there are the same number of advancing points and receding points the number is n. Therefore we have $\int_0^T\int_{\partial\mathcal{G}} \cos\theta_s(y_1)\frac{\partial(3\phi-\phi^3)/4}{\partial y_1}\mathrm{d}y_1\mathrm{d}t \approx \sum_{i=1}^n \int_0^T \big(\cos\theta_s(y_{r,i}(t)) - \cos\theta_s(y_{a,i}(t))\big)dt$.The equation can also be derived by asymptotic inner expansions near the moving contact points[22]. Due to stick-slip effect of the contact point, we have $\theta_s(y_{r,i}(t)) \approx \theta_b$ and $\theta_s(y_{a,i}(t)) \approx \theta_a$ in most of time([22–24]). This leads to

$$\frac{4\sqrt{2}}{3}\mathsf{B}U\int_0^T\int_{\partial\mathcal{G}} \cos\theta_s(y_1)\frac{\partial(3\phi-\phi^3)/4}{\partial y_1}\mathrm{d}y_1\mathrm{d}t \approx \frac{4\sqrt{2}}{3}n\lambda\mathsf{B}UT. \quad (26)$$

Here $\lambda = \cos\theta_b - \cos\theta_a$ depends only on the wetting properties(Young's angles) of pore cell.

Equations (23)- (24) and (26) can be combined to yield

$$FU = U^2/k + F_0 U, \quad (27)$$

or equivalently a force-velocity relation

$$U = k(F - F_0). \quad (28)$$

where the permeability k is the same as that for the homogeneous surfaces given in (20) and $F_0 = \frac{4\sqrt{2}}{3}n\lambda\mathsf{B}/(hL_x)$ is an extra de-pinning force due to the interface tension and chemically roughness of the surface. $\lambda = (\cos\theta_b - \cos\theta_a)$ is the wetting hysteresis property of the two-phase flow on the chemically patterned pore surface, and B is a dimensionless parameter of the two-phase flow(inverse of the capillary number). Therefore, the de-pinning force depends on the wetting and geometric properties of the pore surface as well as the capillary property of the two-phase flow. It is easy to see that the de-pinning force disappears if the solid surface is homogeneous so that there is no contact angle hysteresis i.e. $\theta_a = \theta_b$. In this case, the formula (28) is reduced to (19).

C. General Discussions

We note that the relation (19) and (28) cannot be derived from the standard Leverett model (1) for two-phase porous media flow on the channel cases. For channel cases with periodic conditions(with homogeneous or chemically patterned), the saturation s_i do not change. Then the relative permeability k_{ri} and capillary pressure p_c in Leverett model will be constants. If we suppose $\eta_i = 1$ and ignore the gravity, then (1) is reduced to

$$v_i = -k_{ri}k_0\nabla p_i, \qquad i = 1, 2.$$

Notice that $\nabla p_1 = \nabla(p_2 + p_c) = \nabla p_2$ and is equal to ∇p. Thus the total velocity(or mixture velocity as we study here)

$$v = v_1 + v_2 = -(k_{r1} + k_{r_2})k_0\nabla p. \tag{29}$$

It is easy to see that the equation (29) derived from standard Leverett model is similar to our equation (19) for homogeneous surface case. However, there are differences for the formula of permeability. In (29) the relative permeability k_{ri} depend only on the saturations. In our formula $k^{-1} = k_0^{-1}(1 + b\cdot n)$, which depends explicitly on the number of the moving contact points, instead of the saturations.

For the chemically patterned surface, the extra de-pinning force is missing in (29). We note that the de-pinning force F_0 has different meaning with the capillary pressure $p_c = 2\gamma\kappa = 4\gamma\cos\theta_e/h$. The capillary pressure is the pressure between two fluid phases and always exists whenever $\theta_e \neq \frac{\pi}{2}$. The de-pinning force exists only when the solid surface is inhomogeneous and there is contact angle hysteresis. Physically, the de-pinning force is related to the extra dissipation generated by stick-slip behaviour when the solid surface is chemically patterned[23, 25].

Our analysis in this paper is only for the channel pores, which corresponding to parallel layer flows in two dimensions. The generalization of present approach to other pore geometry and three dimensions is highly nontrivial. However, the energy-dissipation relation (11) obtained from our analysis might have some hint for further studies. From (27), we have the conclusion that the dissipation

$$\mathcal{R} = F_0U + k^{-1}U^2. \tag{30}$$

where the first term is the dissipation by the de-pinning force of contact lines due to the inhomogeneous of the solid surface, and the second term is the viscous dissipation, which includes also a contribution from the contact line slip. We expect that in some general cases, e.g. in a representing volume where two-phase flows mixed up, the dissipation has a similar form to (30) where F_0 and k might be vectors and tensors depending on the effective length of the contact lines which may also depend on the moving direction. In our understandings, it should be the projection of the moving contact lines on transverse direction of flows. In this case, similar relation as (19) and (28) should still hold. Similar to (21), the Darcy's relation (19) becomes

$$\nabla p \propto k^{-1}U \propto k_0^{-1}(1 + b\cdot n)U, \tag{31}$$

with b depends only on the pore geometry and properties of two-phase flow, and n is the effective length of contact lines in three dimension.

The above scaling behavior (31) is consistent with the experimental results in Tallakstad *at el.*[15, 16]. They observed the linear growth of the pressure jump with respect to time for a fixed velocity U (or capillary number $C_a = \frac{\mu_w a^2 v_w}{\gamma\kappa_0} \propto U$) as the front moves in the box. This means the inverse of the permeability increases linearly. This is consistent with (31). As the front moves to the right, the total area of interfaces and the total length n of the contact line increases. Furthermore, they found that the pressure jump $\Delta p \propto \sqrt{U}$(or equivalently $\sqrt{C_a}$) in the steady states. This clearly implies that $k^{-1} \propto U^{-1/2}$(or $k \propto \sqrt{C_a}$ as stated in[15]) This highly nontrivial behavior could be interpreted that the total length of contact lines $n = Nl_x^* \propto C_a^{-1/2}$, where N is the number of nonwetting pores and l_x^* being the characteristic length of the pore in the transverse direction of the flows. The scaling is true from the statistic data on total number of N and the pore size l_x^* in that paper. We note that the experimental results have been explained in a different way in [15].

Finally, we would say that there is still a long way to give a complete model for two-phase flow in porous media. In our analysis, we assume the two-phase flow is mixed in a representing volume and the velocity is small. The analysis will be different if there are macroscopic interfaces. For example, for pure imbibition or pure drainage process, the two-phase fluid is well-separated and the capillary pressure will play an important role. Nevertheless, we think that the analysis for channel flow including moving contact lines might be useful in a pore-network model, which is a good start to understand more general porous media flows.

IV. NUMERICAL VERIFICATIONS

In this section, we carry out some numerical experiments. We solve the problem (13-14) by a finite difference scheme developed in [17, 26]. In our numerical experiments, we set $L_x = 100$, $h = 40$ and $\delta = 1$. The physical parameters are chosen as $\mathsf{R_e} = 0.03$, $\mathsf{B} = 12$, $\mathsf{L_d} = 5$, $\mathsf{V_s} = 5$ [17]. We set the initial velocity as $\mathbf{v}(\mathbf{y}, 0) = \mathbf{0}$, $p(\mathbf{y}, 0) = 0$ and the initial phase function as

$$\phi(\mathbf{y}, 0) = \begin{cases} \tanh((0.3L_x - y_1)/\sqrt{2}) & \text{if } y_1 \le 0.5L_x; \\ \text{than}((y_1 - 0.7L_x)/\sqrt{2}) & \text{otherwise.} \end{cases}$$

The periodic boundary condition are used at the left and right boundaries. In our experiments, we use uniform

meshes with space stepsizes $h_1 = 100/256$ on y_1 direction and $h_2 = 40/64$ in y_2 direction. Time step is choose properly as $dt = 0.035\min(h_1, h_2)^2/(4\mathsf{L_d})$.

A. The chemically homogeneous surface

We consider the chemically homogeneous channel boundary with a static Young's angle $\theta_s = 90°$. We carry out numerical experiments for interface motion under constant force $\mathbf{F} = (F, 0)$. Different values of

$$F = -0.03, -0.02, -0.01, -0.005, -0.0025, -0.00125$$

and different slip length $l_s = 3.2, 1.6, 0.8, 0.4$ are used.

Figure 4 shows a typical horizontal velocity contour and the slip velocity profile when slip length $l_s = 0.4$ and the force $F = 0.01$. It is clearly seen that the slip region near the contact line will contribute significantly to the integral in the right hand side of (17). Figure 5 shows the averaged horizontal velocity U as a function of time. It is easy to see that the horizontal velocity becomes constant after some time. The averaged vertical velocity is always zero and is not shown here. This implies that the flow tends to a traveling wave.

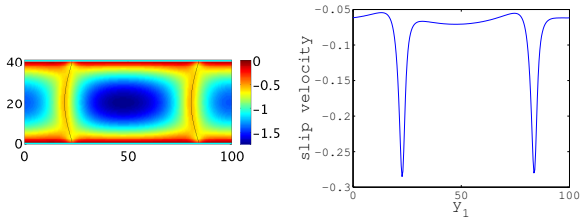

FIG. 4. A typical velocity contour(left) and slip velocity profile(right).(color online)

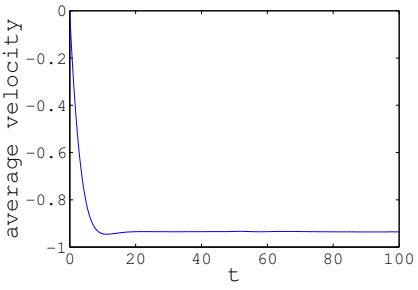

FIG. 5. Spacial Average velocity vs. time($ls = 0.4, F = -0.01$).

The force-velocity relation $U = kF$ is clearly verified in Figure 6. The estimated permeability k in each case is shown in the first row of Table I. In the second row, we show the permeability for one-phase channel computed by $k_0 = h(h + 6l_s)/12$. It is easy to see that the permeability for the two-phase flow is significantly reduced comparing to that of one-phase flow in agreement with our analysis.

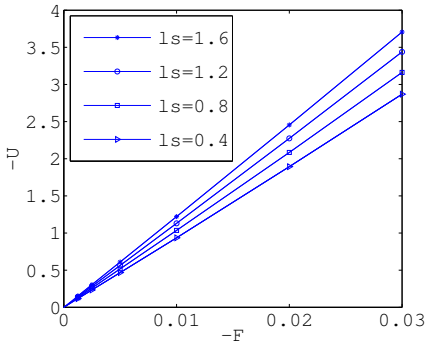

FIG. 6. Darcy's relation for two-phase channel flow with homogeneous boundary

TABLE I. Permeability:two-phase flow v.s. one phase flow

	$l_s = 1.6$	$l_s = 1.2$	$l_s = 0.8$	$l_s = 0.4$
k	122.10	113.01	103.54	93.57
k_0	165.33	157.33	149.33	141.33

B. The chemically patterned surface

We also carry out numerical experiments for chemically patterned channel boundary. We assume that the top and bottom boundaries have the same periodic pattern as shown in Figure 3 with the static Young's angles θ_s and $\pi - \theta_s$, respectively. We consider two cases for $\theta = 80^o$ and $\theta = 60^o$. Similar to the homogeneous case, we simulate interface motion under different external force. In these computations, we set $l_s = 0.4$.

Figure 7 shows some typical horizontal velocity contour and the slip velocity profile when $\theta_s = 80^o$ and the force $F = 0.01$. The large slip behavior near the contact line is clearly shown again. Figure 8 shows the advancing contact angle and receding contact angle as a function of time. It is clearly seen that the advancing contact angle is oscillating around $180^o - \theta_s = 100^o$, and the receding angle is changing around $\theta_s = 80^o$. Figure 9 shows the space averaged horizontal velocity $\tilde{U}(t) = \int_{\mathcal{B}} v_1 dy_1 dy_2$ as function of time. It is easy to see that $\tilde{U}(t)$ becomes periodic in time. The averaged vertical velocity is always zero (not shown here). This implies that the flow becomes periodic in time. In Figure 10, we show the relation between the values of the averaged velocity U(averaged in both space and time) and the values of the external force F for two different contact angles. The Non-Darcy behavior (28) is clearly shown. In this experiment, when F is too small, the numerical errors will affect the numerical results and makes values slightly deviate from the theoretical predictions.

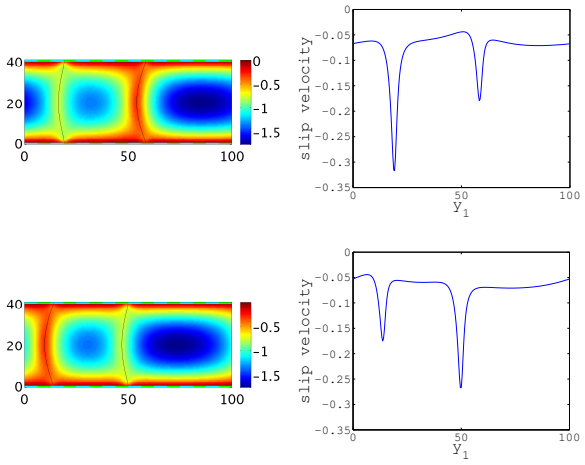

FIG. 7. Some typical velocity contours and slip velocity profile($\theta_s = 80^o, F = -0.01$).(color online)

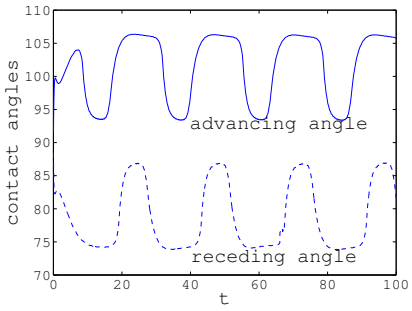

FIG. 8. Advancing contact angle and receding contact angle($\theta_s = 80^o, F = -0.01$).

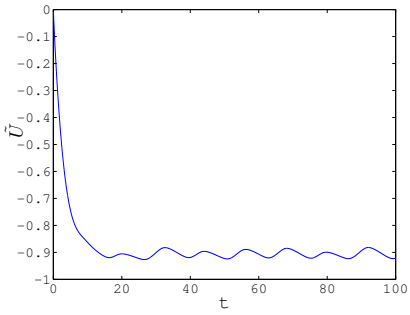

FIG. 9. Spacial average velocity vs. time($\theta_s = 80^o, F = -0.01$).

V. CONCLUSION REMARKS

In conclusion, channel flows constitute probably the most elementary component of any considerations about porous media flows. Hence the permeability dependence on moving contact lines and the non-Darcy behavior induced by chemical or geometric roughness should persist in the general problem of multiphase permeability of porous media. In particular, our result offers a quantitatively understanding of the prior observation of non-Darcy behavior in either simulations or experiments [23–25, 27, 28] that involved contact line motion. Here the extra force F_0 can be especially important at low flow rates, representing the dissipation caused by the contact lines when each crosses from one region of the contact angle to another. Such considerations have been missing in previous considerations of multiphase permeability, and its inclusion may enhance the realism of the modeling effort. Finally, the generalization of the analysis in this paper to other pore geometry and three-dimensional models is highly non-trivial. We expect that the energy dissipation relation and the analysis for channel flows might be helpful in simple pore network model.

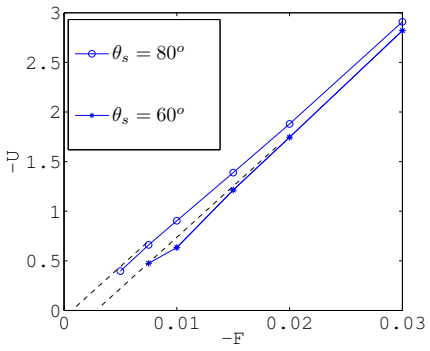

FIG. 10. Force-velocity relation for two-phase channel flow with periodic patterned boundary

Acknowledgments: We thank Ping Sheng for many illuminating discussions. This publication was based on work supported in part by Hong Kong RGC-GRF Grants 605513, 605311, and by NSFC 11001260.

[1] H. Darcy, *Les Fontaines Publiques de la Ville de Dijon* (Dalmont, Paris, 1856).
[2] J. Keller, Lecture Notes in Pure and Appl. Math. **54**, 429 (1980).
[3] E. Sanchez-Palencia, *Nonhomogeneous media and vibration theory*, 127 (Springer-Verlag, Berilin, New York, 1980).
[4] U. Hornung, *Homogenization and Porous Media* (Springer, 1997).
[5] W. Gray and K. O'Neill, Water Resour. Res. **12**, 148 (1976).
[6] S. Whitaker, Transp. Porous Med. **1**, 3 (1986).
[7] J. Bear, *Dynamics of Fluids in Porous Media* (Elsevier, New York, 1988).

[8] M. Hassanizadeh, Porous Med. **9**, 207 (1986).
[9] M. Balhoff, A. Mikelić, and F. Wheeler, Transp. Porous Med. **81**, 35 (2010).
[10] M. Leverett, Trans. AIME **142**, 152 (1941).
[11] J. Stokes, D. Weitz, J. Gollub, A. Dougherty, M. Robbins, P. Chaikin, and H. Lindsay, Phys. Rev. Lett. **57**, 1718 (1986).
[12] D. G. Avraam and A. Payatakes, Journal of Fluid Mechanics **293**, 207 (1995).
[13] D. G. Avraam and A. C. Payatakes, in *Multiphase Flow in Porous Media* (Springer, 1995) pp. 135–168.
[14] C. Tsakiroglou, D. G. Avraam, and A. Payatakes, Advances in water resources **30**, 1981 (2007).
[15] K. T. Tallakstad, G. Løvoll, H. A. Knudsen, T. Ramstad, E. G. Flekkøy, and K. J. Måløy, Physical Review E **80**, 036308 (2009).
[16] K. T. Tallakstad, H. A. Knudsen, T. Ramstad, G. Løvoll, K. Måløy, R. Toussaint, and E. G. Flekkøy, Physical review letters **102**, 074502 (2009).
[17] T. Qian, X.-P. Wang, and P. Sheng, Phys. Rev. E **68**, 016306 (2003).
[18] T. Qian, X.-P. Wang, and P. Sheng, J. Fluid Mech. **564**, 333 (2006).
[19] T. Qian, X.-P. Wang, and P. Sheng, Phys. Rev. lett. **63**, 094501 (2004).
[20] L. Hocking, Journal of Fluid Mechanics **79**, 209 (1977).
[21] M. Gao, "Ph.d thesis," (2012).
[22] X. Xu and X.-P. Wang, SIAM J. Appl. Math. **71**, 1753 (2011).
[23] X.-P. Wang, T. Qian, and P. Sheng, J. Fluid Mech. **605**, 59 (2008).
[24] W. Ren and W. E, Physics of Fluids **23**, 072103 (2011).
[25] J. Joanny and M. Robbins, J. Chem. Phys **92**, 32063212 (1990).
[26] M. Gao and X. Wang, J. Comput. Phys. **231**, 1372 (2012).
[27] E. Schaffer and P.-Z. Wong, Phys. Rev. E **61**, 5257 (2000).
[28] P. Sheng and M. Zhou, Phys. Rev. A **45**, 5694 (1992).
[29] X.-P. Wang and Y.-G. Wang, Methods and Applications of Analysis **14**, 287 (2007).

Appendix A: Calculations

1. The expansions

Substitute the expansions in Section II.B into the equations (6)-(7), we have

$$\begin{cases} \frac{1}{\varepsilon}\frac{\partial}{\partial s}(\phi_0+\varepsilon\phi_1+\cdots) \\ +(\mathbf{v}_0+\varepsilon\mathbf{v}_1+\cdots)\cdot(\nabla_x+\varepsilon^{-1}\nabla_y)(\phi_0+\varepsilon\phi_1+\cdots) \\ =\varepsilon^2\mathsf{L_d}(\Delta_x+2\varepsilon^{-1}(\nabla_x\cdot\nabla_y)+\varepsilon^{-2}\Delta_y)(\varepsilon^{-1}\mu_0+\mu_1+\cdots), \\ \varepsilon\mathsf{R_e}\Big[\frac{1}{\varepsilon}\frac{\partial\mathbf{v}}{\partial s}+(\mathbf{v}_0+\varepsilon\mathbf{v}_1+\ldots)(\nabla_x+\frac{1}{\varepsilon}\nabla_y)(\mathbf{v}_0+\varepsilon\mathbf{v}_1+\cdots)\Big] \\ =\mathbf{F}-(\nabla_x+\varepsilon^{-1}\nabla_y)(p_0+\varepsilon p_1+\cdots) \\ +\varepsilon^2(\Delta_x+2\varepsilon^{-1}(\nabla_x\cdot\nabla_y)+\varepsilon^{-2}\Delta_y)(\mathbf{v}_0+\varepsilon\mathbf{v}_1+\cdots) \\ +\varepsilon^2\mathsf{B}(\varepsilon^{-1}\mu_0+\mu_1+\cdots)(\nabla_x+\varepsilon^{-1}\nabla_y)(\phi_0+\varepsilon\phi_1+\cdots), \\ (\nabla_x+\varepsilon^{-1}\nabla_y)\cdot(\mathbf{v}_0+\varepsilon\mathbf{v}_1+\cdots)=0, \end{cases} \tag{A1}$$

with boundary conditions

$$\begin{cases} \varepsilon[\frac{1}{\varepsilon}\frac{\partial}{\partial s}(\phi_0+\varepsilon\phi_1+\cdots) \\ \quad +(v_{0,\tau}+\varepsilon v_{1,\tau}+\cdots)(\nabla_x+\varepsilon^{-1}\nabla_y)(\phi_0+\varepsilon\phi_1+\cdots)\cdot\tau] \\ =-\mathsf{V_s}(\mathcal{L}_0(\phi_0)+O(\varepsilon)), \\ {l_s}^{-1}(v_{0,\tau}+\varepsilon v_{1,\tau}+\cdots) \\ =-\varepsilon(\nabla_x+\varepsilon^{-1}\nabla_y)(v_{0,\tau}+\varepsilon v_{1,\tau}+\cdots)\cdot\mathbf{n} \\ \qquad +\varepsilon\mathsf{B}(\mathcal{L}_0(\phi_0)+O(\varepsilon))(\nabla_x+\varepsilon^{-1}\nabla_y)(\phi_0+\varepsilon\phi_1+\cdots)\cdot\tau, \\ (\nabla_x+\varepsilon^{-1}\nabla_y)(\varepsilon^{-1}\mu_0+\mu_1+\cdots)\cdot\mathbf{n}=0, \\ (\mathbf{v}_0+\varepsilon\mathbf{v}_1+\cdots)\cdot\mathbf{n}=0, \end{cases} \tag{A2}$$

The leading orders of the the equation will gives (8)-(10).

2. Derivation of the Dissipation function

We now multiply $\mathbf{v}_0$ to the first equation of (9) and integrate in $\mathcal{B}$. This leads to

$$\int_{\mathcal{B}}\mathsf{R_e}[\frac{\partial\mathbf{v}_0}{\partial s}\cdot\mathbf{v}_0+(\mathbf{v}_0\cdot\nabla_y)\mathbf{v}_0\cdot\mathbf{v}_0]\mathrm{d}\mathbf{y}=(\mathbf{F}-\nabla P(\mathbf{x}))\cdot\int_{\mathcal{B}}\mathbf{v}_0\mathrm{d}\mathbf{y} + \int_{\mathcal{B}}[-\nabla_y p_1\cdot\mathbf{v}_0+\Delta_y\mathbf{v}_0\cdot\mathbf{v}_0+\mathsf{B}\mu_0\nabla_y\phi_0\cdot\mathbf{v}_0]\mathrm{d}\mathbf{y} \tag{A3}$$

We have denoted $\nabla P(x)=\nabla_x p_0(x)$. The first term on the left hand side is given by

$$\mathsf{R_e}\int_{\mathcal{B}}\frac{\partial\mathbf{v}_0}{\partial s}\cdot\mathbf{v}_0\mathrm{d}\mathbf{y}=\frac{\mathsf{R_e}}{2}\frac{\partial}{\partial s}\int_{\mathcal{B}}|\mathbf{v}_0|^2\mathrm{d}\mathbf{y} \tag{A4}$$

The second term on the left hand side of (A3) is calculated as

$$\mathsf{R_e}\int_{\mathcal{B}}(\mathbf{v}_0\cdot\nabla_y)\mathbf{v}_0\cdot\mathbf{v}_0\mathrm{d}\mathbf{y}=\frac{\mathsf{R_e}}{2}\int_{\mathcal{B}}(\mathbf{v}_0\cdot\nabla_y)|\mathbf{v}_0|^2\mathrm{d}\mathbf{y} =\frac{\mathsf{R_e}}{2}\int_{\partial\mathcal{B}}(\mathbf{v}_0\cdot\mathbf{n})|\mathbf{v}_0|^2\mathrm{d}\sigma_y-\frac{\mathsf{R_e}}{2}\int_{\partial\mathcal{B}}(\nabla_y\cdot\mathbf{v}_0)|\mathbf{v}_0|^2\mathrm{d}\mathbf{y}=0. \tag{A5}$$

Here $\mathrm{d}\sigma_y$is the line integral variable along the boundary of $\partial\mathcal{G}$. In the derivation, we use the divergence free condition of $\mathbf{v}_0$, the zero normal velocity boundary condition on $\partial\mathcal{G}$ and the periodic boundary condition of $\mathbf{v}_0$ on $\partial\mathcal{Y}$. Similarly, the second term on the right hand side of (A3) is given by

$$-\int_{\mathcal{B}}\nabla_y p_1\cdot\mathbf{v}_0\mathrm{d}\mathbf{y}=-\int_{\partial\mathcal{B}}p_1\mathbf{v}_0\cdot\mathbf{n}\mathrm{d}\sigma_y+\int_{\mathcal{B}}p_1\nabla_y\cdot\mathbf{v}_0\mathrm{d}\mathbf{y}=0. \tag{A6}$$

The third term on the right hand side of (A3) is given by

$$\begin{aligned}\int_{\mathcal{B}}\Delta_y\mathbf{v}_0\cdot\mathbf{v}_0\mathrm{d}\mathbf{y}&=\int_{\partial\mathcal{B}}(\mathbf{n}\cdot\nabla_y)\mathbf{v}_0\cdot\mathbf{v}_0\mathrm{d}\sigma_y-\int_{\mathcal{B}}|\nabla_y\mathbf{v}_0|^2\mathrm{d}\mathbf{y} \\ &=\int_{\partial\mathcal{G}}(\nabla_y v_{0,\tau}\cdot\mathbf{n})v_{0,\tau}\mathrm{d}\sigma_y-\int_{\mathcal{B}}|\nabla_y\mathbf{v}_0|^2\mathrm{d}\mathbf{y} \\ &=-l_s^{-1}\int_{\partial\mathcal{G}}v_{0,\tau}^2\mathrm{d}\sigma_y+\mathsf{B}\int_{\partial\mathcal{G}}\mathcal{L}_0(\phi_0)\nabla_y\phi_0\cdot\tau v_{0,\tau}\mathrm{d}\sigma_y \\ &\quad-\int_{\mathcal{B}}|\nabla_y\mathbf{v}_0|^2\mathrm{d}\mathbf{y}.\end{aligned} \tag{A7}$$

Here we use the slip boundary conditions in (10) in addition to other boundary conditions of $\mathbf{v}_0$. The second term in (A7) could be further computed as

$$\begin{aligned}&\mathsf{B}\int_{\partial\mathcal{G}}\mathcal{L}_0(\phi_0)\nabla_y\phi_0\cdot\tau v_{0,\tau}\mathrm{d}\sigma_y=\mathsf{B}\int_{\partial\mathcal{G}}\mathcal{L}_0(\phi_0)(\dot{\phi}_0-\frac{\partial\phi_0}{\partial s})\mathrm{d}\sigma_y\\&=-\frac{\mathsf{B}}{\mathsf{V}_s}\int_{\partial\mathcal{G}}\dot{\phi}_0^2\mathrm{d}\sigma_y-\mathsf{B}\int_{\partial\mathcal{G}}\mathcal{L}_0(\phi_0)\frac{\partial\phi_0}{\partial s}\mathrm{d}\sigma_y\end{aligned}\tag{A8}$$

The last term in the right hand side of (A3) is calculated as

$$\begin{aligned}&\int_{\mathcal{B}}\mathsf{B}\mu_0\nabla_y\phi_0\cdot\mathbf{v}_0\mathrm{d}\mathbf{y}=\int_{\mathcal{B}}\mathsf{B}\mu_0(\mathsf{L_d}\Delta_y\mu_0-\frac{\partial\phi_0}{\partial s})\mathrm{d}\mathbf{y}\\&=\mathsf{B}\mathsf{L_d}\int_{\partial\mathcal{B}}\mu_0\nabla_y\mu_0\cdot\mathbf{n}\mathrm{d}\sigma_y-\mathsf{B}\mathsf{L_d}\int_{\mathcal{B}}|\nabla\mu_0|^2\mathrm{d}\mathbf{y}\\&\quad-\mathsf{B}\int_{\mathcal{B}}\mu_0\frac{\partial\phi_0}{\partial s}\mathrm{d}\mathbf{y}\\&=-\mathsf{B}\mathsf{L_d}\int_{\partial\mathcal{B}}|\nabla\mu_0|^2\mathrm{d}\mathbf{y}-\mathsf{B}\int_{\mathcal{B}}\mu_0\frac{\partial\phi_0}{\partial s}\mathrm{d}\mathbf{y}\end{aligned}\tag{A9}$$

Finally, direct computations gives

$$\begin{aligned}&-\mathsf{B}\int_{\partial\mathcal{G}}\mathcal{L}_0(\phi_0)\frac{\partial\phi_0}{\partial s}\mathrm{d}\sigma_y=-\mathsf{B}\delta\int_{\partial\mathcal{G}}\nabla_y\phi_0\cdot\mathrm{n}\frac{\partial\phi_0}{\partial s}\mathrm{d}\sigma_y\\&\qquad-\mathsf{B}\frac{\partial}{\partial s}\int_{\partial\mathcal{G}}\gamma_{wf}(\phi_0)\mathrm{d}\sigma_y;\end{aligned}\tag{A10}$$

$$\begin{aligned}&-\mathsf{B}\int_{\mathcal{B}}\mu_0\frac{\partial\phi_0}{\partial s}\mathrm{d}\mathbf{y}=\mathsf{B}\delta\int_{\partial\mathcal{G}}\nabla_y\phi_0\cdot\mathrm{n}\frac{\partial\phi_0}{\partial s}\mathrm{d}\sigma_y\\&\quad-\frac{\mathsf{B}\delta}{2}\frac{\partial}{\partial s}\int_{\mathcal{B}}|\nabla_y\phi_0|^2\mathrm{d}\mathbf{y}-\frac{\mathsf{B}}{\delta}\frac{\partial}{\partial s}\int_{\mathcal{B}}\frac{(1-\phi_0^2)^2}{4}\mathrm{d}\mathbf{y}\end{aligned}\tag{A11}$$

Combine all the terms, we have

$$\begin{aligned}&(\mathbf{F}-\nabla P(\mathbf{x}))\cdot\int_{\mathcal{B}}\mathbf{v}_0\mathrm{d}\mathbf{y}\\&=\int_{\mathcal{B}}|\nabla\mathbf{v}_0|^2\mathrm{d}\mathbf{y}+\int_{\partial\mathcal{G}}\frac{v_{0,\tau}^2}{l_s}\mathrm{d}\sigma_y+\frac{\mathsf{B}}{\mathsf{V_s}}\int_{\partial\mathcal{G}}\dot{\phi_0}^2\mathrm{d}\sigma_y\\&\quad+\mathsf{B}\mathsf{L_d}\int_{\mathcal{B}}|\nabla\mu_0|\mathrm{d}\mathbf{y}+\frac{\partial}{\partial s}\Big[\mathsf{R_e}\int_{\mathcal{B}}\frac{|\mathbf{v}_0|^2}{2}\mathrm{d}\mathbf{y}\\&\qquad+\mathsf{B}\int_{\partial\mathcal{G}}\gamma_{wf}(\phi_0)\mathrm{d}\sigma_y+\mathsf{B}\int_{\mathcal{B}}\big(\frac{\delta}{2}|\nabla\phi_0|^2+\frac{1}{\delta}f(\phi_0)\big)\mathrm{d}\mathbf{y}\Big].\end{aligned}\tag{A12}$$

with $f(\phi)=(1-\phi^2)^2/4$. We then integrate the above equation in fast time s in (0,T), and notice the assumption of time periodicity, we have (11).

3. Computations in homogeneous channel

We multiply $\mathbf{U}$ to the first equation of (15) and integrate in $\mathcal{B}$. We have

$$\begin{aligned}\mathbf{F}\cdot\mathbf{U}|\mathcal{B}|=&\mathsf{R_e}\int_{\mathcal{B}}\big((\mathbf{v}-\mathbf{U})\cdot\nabla\big)\mathbf{v}\cdot\mathbf{U}\mathrm{d}\mathbf{y}\\&-\int_{\mathcal{B}}(-\nabla p+\Delta\mathbf{v}+\mathsf{B}\mu\nabla\phi)\cdot\mathbf{U}\mathrm{d}\mathbf{y}\end{aligned}\tag{A13}$$

The first term on the right hand side becomes

$$\begin{aligned}&\mathsf{R_e}\int_{\mathcal{B}}\big((\mathbf{v}-\mathbf{U})\cdot\nabla\big)\mathbf{v}\cdot\mathbf{U}\mathrm{d}\mathbf{y}=\mathsf{R_e}U\int_{\mathcal{B}}(\mathbf{v}-\mathbf{U})\cdot\nabla v_1\mathrm{d}\mathbf{y}\\&=-\mathsf{R_e}U\int_{\mathcal{B}}v_1\nabla\cdot\mathbf{v}\mathrm{d}\mathbf{y}+\mathsf{R_e}U\int_{\partial\mathcal{G}}(\mathbf{v}-\mathbf{U})\cdot\mathbf{n}v_1\mathrm{d}\sigma_y\\&\quad+\mathsf{R_e}U\Big(\int_{\{y_1=L_x\}}(v_1-U)v_1\mathrm{d}y_2-\int_{\{y_1=0\}}(v_1-U)v_1\mathrm{d}y_2\Big)\\&=0.\end{aligned}\tag{A14}$$

Here we have used the periodic condition of $\mathbf{v}$ at $y_1=0,L_x$ in addition to the boundary condition of $\mathbf{v}$ on $\partial\mathcal{G}$ as well as the divergence-free property of $\mathbf{v}$ in $\mathcal{B}$. Integration by part again, the second term of the right hand side of (A13) reads

$$\begin{aligned}\int_{\mathcal{B}}\nabla p\cdot\mathbf{U}\mathrm{d}\mathbf{y}=&\int_{\partial\mathcal{G}}p\mathbf{U}\cdot\mathbf{n}\mathrm{d}\sigma_y+\int_{\{y_1=L_x\}}pU\mathrm{d}y_2\\&-\int_{\{y_1=0\}}pU\mathrm{d}y_2=0.\end{aligned}\tag{A15}$$

This is simply from the periodic boundary condition of p at $y_1=0,L_x$. The third term of the right hand side of (A13) gives

$$\begin{aligned}&-\int_{\mathcal{B}}\Delta\mathbf{v}\cdot\mathbf{U}\mathrm{d}\mathbf{y}=-\int_{\partial\mathcal{G}}\frac{\partial\mathbf{v}}{\partial\mathbf{n}}\cdot\mathbf{U}\mathrm{d}s_y-\int_{\{y_1=L_x\}}\frac{\partial\mathbf{v}}{\partial\mathbf{n}}\cdot\mathbf{U}\mathrm{d}y_2\\&\qquad-\int_{\{y_1=0\}}\frac{\partial\mathbf{v}}{\partial\mathbf{n}}\cdot\mathbf{U}\mathrm{d}y_2\\&=-U\int_{\partial\mathcal{G}}\frac{\partial v_\tau}{\partial\mathbf{n}}\mathrm{d}\sigma_y=U\int_{\partial\mathcal{G}}\frac{v_\tau}{l_s}\mathrm{d}\sigma_y-\mathsf{B}U\int_{\partial\mathcal{G}}L(\phi)\frac{\partial\phi}{\partial\tau}\mathrm{d}\sigma_y\\&=U\int_{\partial\mathcal{G}}\frac{v_\tau}{l_s}\mathrm{d}\sigma_y-\delta\mathsf{B}U\int_{\partial\mathcal{G}}\frac{\partial\phi}{\partial\mathbf{n}}\frac{\partial\phi}{\partial\tau}\mathrm{d}\sigma_y\\&\quad-\frac{\sqrt{2}\mathsf{B}U\cos\theta_s}{6}\int_{\partial\mathcal{G}}\frac{\partial(3\phi-\phi^3)}{\partial y_1}\mathrm{d}y_1\\&=U\int_{\partial\mathcal{G}}\frac{v_\tau}{l_s}\mathrm{d}\sigma_y-\delta\mathsf{B}U\int_{\partial\mathcal{G}}\frac{\partial\phi}{\partial\mathbf{n}}\frac{\partial\phi}{\partial\tau}\mathrm{d}\sigma_y.\end{aligned}\tag{A16}$$

Here in the second equation, we use the periodic condition of $\mathbf{v}$ on $y_1=0,L_x$. In the third equation, we have used the generalized Navier condition on $\partial\mathcal{G}$, and in the fourth equation we have used the fact that θ_s is a constant on the homogeneous surface and ϕ is periodic. The

last term in equation (A13) can be calculated as

$$
\begin{aligned}
&-\mathsf{B}\int_{\mathcal{B}}\mu\nabla\phi\cdot\mathbf{U}\mathrm{d}\mathbf{y}=-\mathsf{B}U\int_{\mathcal{B}}(-\delta\Delta\phi-\frac{\phi-\phi^3}{\delta})\frac{\partial\phi}{\partial y_1}\mathrm{d}\mathbf{y}\\
&=\delta\mathsf{B}U\int_{\partial\mathcal{G}}\frac{\partial\phi}{\partial\mathbf{n}}\frac{\partial\phi}{\partial y_1}\mathrm{d}\sigma_y\\
&\quad-\frac{\mathsf{B}U}{\delta}\int_{\mathcal{B}}\delta^2\nabla\phi\cdot\nabla\partial_{y_1}\phi+(\phi-\phi^3)\partial_{y_1}\phi\mathrm{d}\mathbf{y}\\
&=\delta\mathsf{B}U\int_{\partial\mathcal{G}}\frac{\partial\phi}{\partial\mathbf{n}}\frac{\partial\phi}{\partial\tau}\mathrm{d}\sigma_y\\
&\quad-\frac{\mathsf{B}U}{\delta}\int_{\mathcal{B}}\delta^2\partial_{y_1}|\nabla\phi|^2+\partial_{y_1}\frac{(1-\phi^2)^2}{4}\mathrm{d}\mathbf{y}\\
&=\delta\mathsf{B}U\int_{\partial\mathcal{G}}\frac{\partial\phi}{\partial\mathbf{n}}\frac{\partial\phi}{\partial\tau}\mathrm{d}\sigma_y \qquad \text{(A17)}
\end{aligned}
$$

Combining equations (A13)-(A17), we have

$$\mathbf{F}\cdot\mathbf{U}|\mathcal{B}|=U\int_{\partial\mathcal{G}}l_s^{-1}v_\tau\mathrm{d}\sigma_y. \qquad \text{(A18)}$$

This further leads to (17).

4. Computations in chemically pattern channel

We first estimate each term on the right hand side of (22). The computations are similar to that in the previous subsection. Direct computations give that

$$
\begin{aligned}
&\mathsf{Re}\int_{\mathcal{B}}(\partial_t\mathbf{v}\cdot\mathbf{U}+(\mathbf{v}\cdot\nabla)\mathbf{v}\cdot\mathbf{U})\mathrm{d}\mathbf{y}\\
&=\mathsf{Re}U\int_{\mathcal{B}}\partial_t v_1\mathrm{d}\mathbf{y}=\mathsf{Re}U\partial_t\int_{\mathcal{B}}v_1\mathrm{d}\mathbf{y}. \qquad \text{(A19)}
\end{aligned}
$$

For the second term, we have

$$\int_{\mathcal{B}}\nabla p\cdot\mathbf{U}\mathrm{d}\mathbf{y}=0. \qquad \text{(A20)}$$

For the third term, we have

$$
\begin{aligned}
&-\int_{\mathcal{B}}\Delta\mathbf{v}\cdot\mathbf{U}\mathrm{d}\mathbf{y}=-U\int_{\partial\mathcal{G}}\frac{\partial v_\tau}{\partial\mathbf{n}}\mathrm{d}\sigma_y\\
&=U\int_{\partial\mathcal{G}}l_s^{-1}v_\tau\mathrm{d}\sigma_y-\delta\mathsf{B}U\int_{\partial\mathcal{G}}\frac{\partial\phi}{\partial\mathbf{n}}\frac{\partial\phi}{\partial\tau}\mathrm{d}\sigma_y\\
&\quad-\frac{\sqrt{2}}{6}\mathsf{B}U\int_{\partial\mathcal{G}}\cos\theta_s(y_1)\frac{\partial(3\phi-\phi^3)}{\partial y_1}\mathrm{d}y_1. \qquad \text{(A21)}
\end{aligned}
$$

The last term in (22) yields

$$-\mathsf{B}\int_{\mathcal{B}}\mu\nabla\phi\cdot\mathbf{U}\mathrm{d}\mathbf{y}=\delta\mathsf{B}U\int_{\partial\mathcal{G}}\frac{\partial\phi}{\partial\mathbf{n}}\frac{\partial\phi}{\partial\tau}\mathrm{d}\sigma_y \qquad \text{(A22)}$$

Combining equations (A19)-(A22), we have

$$
\begin{aligned}
\mathbf{F}\cdot\mathbf{U}|\mathcal{B}|=&\mathsf{R_e}U\partial_t\int_{\mathcal{B}}v_1\mathrm{d}\mathbf{y}+U\int_{\partial\mathcal{G}}l_s^{-1}v_\tau\mathrm{d}\sigma_y\\
&-\frac{\sqrt{2}}{6}\mathsf{B}U\int_{\partial\mathcal{G}}\cos\theta_s(y_1)\frac{\partial(3\phi-\phi^3)}{\partial y_1}\mathrm{d}y_1. \qquad \text{(A23)}
\end{aligned}
$$

Integrating the above equation in time over one period, the left-hand side gives

$$\int_0^T\mathbf{F}\cdot\mathbf{U}|\mathcal{B}|\mathrm{d}t=FU|\mathcal{B}|T=FUL_xhT. \qquad \text{(A24)}$$

The first term on the right-hand side of the equation (A23) gives

$$\mathsf{R}_eU\int_0^T\Big(\partial_t\int_{\mathcal{B}}v_1\mathrm{d}\mathbf{y}\Big)\mathrm{d}t=0. \qquad \text{(A25)}$$

because of the time-periodicity of the velocity. This leads to (23).

Appendix B: Slip profile near the moving contact line

Far from the moving contact line, it is well known that the slip velocity of fluid is relatively small so that a no-slip boundary condition is a good approximation in general. In the vicinity of the moving contact line, near complete-slip has been observed by MD simulations for immiscible flows(see [19] and references therein). The slip profile is studied in the paper[19] by MD simulations and by continuum simulations based on the phase field model (6) with GNBC boundary conditions. It is found that there is a partial slip region spreading from the complete slip region to the nearly no-slip region. In the partial slip region, the ratio of the slip velocity and the macroscopic velocity, v_{slip}/U, has a universal profile which decays in a power law of $1/x$ (see Fig. 11) where x is the distance from the MCL. The outer cutoff for the partial-slip region, denoted by R, is determined by the overall size of the system (the channel height h in our case). The partial slip region has a significant contribution to total dissipations. It is also shown that the universal slip velocity v_{slip} can be approximated by,

$$\frac{v_{slip}}{U}=\frac{1}{1+x/(al_s)}, \qquad \text{(B1)}$$

where $a=2.14$ is obtained by a data fitting approach to the MD experiments results. Based on this, in the integral of the right-hand side of (17), the slip region will contribute a constant:

$$\mathsf{A}=2l_s^{-1}\int_0^{\mathsf{R}}\frac{v_{slip}}{U}\mathrm{d}x=2\times2.14\ln(1+R/(2.14l_s)), \qquad \text{(B2)}$$

which could be very large. For example, if $l_s=1nm$ and $\mathsf{R}=1\mu m$, then $\mathsf{A}\approx36.2$. This might change the permeability significantly, especially when L_x/h is not too big.

Hocking gave an asymptotic analysis to the moving contact line problem [20] assuming the Navier slip boundary condition near MCL, in which the partial-slip profile with a power law $1/x$ is also obtained. The author considered two-phase fluids on a moving solid surface as in

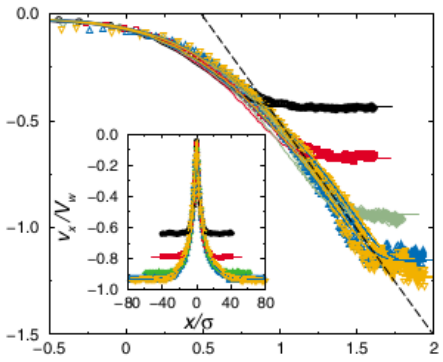

FIG. 11. Scaled slip velocity vs scaled distance from MCL:the log-log sclaling and the original profile(small subfigure)[19].(color online)

Fig. 12. The solid surface has a constant velocity U and the contact line does not move with the boundary. Away from the interface, the system is assumed to be described by Stokes equation with the Navier slip boundary condition. This can also be derived from the sharp interface limit of system (13) and (14) [29]. The inner region is considered by setting $\rho = \ln(x/l_s)$. With the help of stream functions, the author derived the following formula for tangential stess for the two fluids (that is (2.7) in [20]),

$$\tau_1 = \eta_1 U x^{-1} k_1(\rho), \qquad \tau_2 = \eta_2 U x^{-1} k_2(\rho), \qquad \text{(B3)}$$

where η_1 and η_2 are viscositis for the two fluids, k_1 and k_2 are two functions determined by two coupled integral equations(see (2.19) in [20] for the formula). k_1 and k_2 satisfy the following boundary conditions,

$$k_i(\rho) \sim e^{\rho} \text{ as } \rho \to -\infty, \qquad i = 1, 2,$$
$$k_i(\rho) \to \hat{k}_i \text{ as } \rho \to +\infty, \qquad i = 1, 2,$$

where $\hat{k}_i$ are given constants determined by the contact angles and the viscosity ratio. In addition, when the slip region R is large, the friction force due to the moving contact line is approxmated by ((2.28) in [20])

$$f_i(\mathsf{R}) = \int_0^{\mathsf{R}} \tau_i \mathrm{d}x = \eta_i U(\hat{k}_i \ln(\mathsf{R}/l_s) + h_i + o(1)). \qquad \text{(B4)}$$

Here h_i are two values depends on contact angles, viscosity, etc. Some specific values can be found in Table 1 in [20].

Noticing the Navier slip boundary condition $l_s^{-1} v_{i,slip} = \tau_i$, we derive from (B3) that

$$\frac{v_{i,slip}}{U} = \frac{l_s}{x} \eta_i k_i \Big(\ln \frac{x}{l_s} \Big), \qquad i = 1, 2. \qquad \text{(B5)}$$

This implies the slip velocity has a profile given by function k_i. The integral equations for k_i are solved numerically in [21] for a liquid-gas system and the Fig. 13

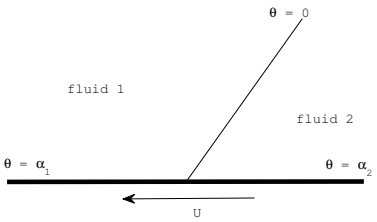

FIG. 12. Two phase fluid with a moving contact line.

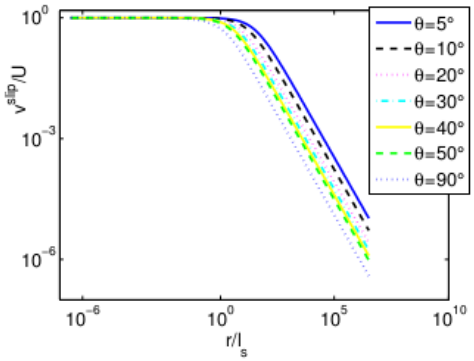

FIG. 13. Scaled slip velocity vs scaled distance from MCL given by asymptotics[21].(color online)

displays the scaled slip velocity and the scaled distance x/l_s in the inner region of MCL for liquid phase and for different contact angles. The power-law behavior of $v_{slip}/U \propto l_s/x$ is clearly shown. From (B4), we can compute the parameter A as

$$\begin{aligned} \mathsf{A} &= \frac{1}{U} \left(\int_0^{\mathsf{R}} l_s^{-1} v_{1,slip} \mathrm{d}x + \int_0^{\mathsf{R}} l_s^{-1} v_{2,slip} \mathrm{d}x \right) \\ &= \frac{1}{U} \left(\int_0^{\mathsf{R}} \tau_1 \mathrm{d}x + \int_0^{\mathsf{R}} \tau_2 \mathrm{d}x \right) \\ &= \sum_{i=1,2} \eta (\hat{k}_i \ln(\mathsf{R}/l_s) + h_i + o(1)). \end{aligned} \qquad \text{(B6)}$$

When R is relative large compared to l_s, A can be significant large, just as shown in [19].